# Corrosion Behavior and Oxide Properties of Zr-Nb-Cu and Zr-Nb-Sn Alloy in High Dissolved Hydrogen Primary Water Chemistry

Yun Ju Lee[a], Taeho Kim[a], and Ji Hyun Kim[a]*
[a] *School of Mechanical and Nuclear Engineering Ulsan National Institute of Science and Technology (UNIST), Ulju-gun, Ulsan 44919, Republic of Korea*
[*] *Corresponding author: kimjh@unist.ac.kr*

## 1. Introduction

Zirconium alloys are used for fuel cladding of pressurized water reactor (PWR), because they have a very low thermal neutron capture cross section and acceptable mechanical properties. And to ensure the safety of nuclear power reactor, the performance and sustainability of nuclear fuel should be understood.

Currently, the water-metal interface is regarded as rate-controlling site governing the rapid oxidation transition in high burn-up fuel [1-4]. And the zirconium oxide is made in water-metal interface and its structure and phase do an important role in terms of oxide properties.

During oxidation process, the protective tetragonal oxide layer develops at the interface due to accumulated high stress during oxide growth, and it turns into non-protective monoclinic oxide with increasing oxide thickness, thus decreasing the stress [5].

It has been reported that Nb addition was proven to be very beneficial for increasing the corrosion resistance of the zirconium alloys. From a more recent study, Cu addition in Nb containing Zirconium alloy was reported to be effective for increasing corrosion resistance in water containing B and Li. According to the previous research conducted, Zr-Nb-Cu shows better corrosion resistance than Zircaloy-4.

The dissolved hydrogen (DH) concentration is the key issue of primary water chemistry, and the effect of DH concentration on the corrosion rate of nickel based alloy has been researched. However, the effect of DH on the zirconium alloy corrosion mechanism was not fully investigated.

In many previous research, it has been shown that the high temperature oxidation of zirconium leads to the growth of an oxide scale which consists in a mixture of tetragonal and monoclinic phases [5]. Tetragonal phase zirconium oxide is stable at high temperature above 1150 ℃, but it has been known that it can be stabilized at lower temperatures in the presence of high compressive stresses [1]. By previous studies, it has been known that stabilized tetragonal phase zirconium oxide can be used as indicator of good corrosion resistance [1-6]. According to previous research, tetragonal phase exists near oxide/metal interface and as the distance from oxide/metal interface increases, monoclinic phase becomes dominant, because compressive stress exists near oxide/metal interface and released as the distance from oxide/metal interface increase [1,5,6].

In this research, the zirconium alloys, Zr-Nb-Cu and Zr-Nb-Sn, are oxidized in high DH concentration, 50 cc/kg. Then, the scanning electron microscopy is used for investigating the oxide growth of zirconium-water interface. And the Raman spectroscopic measurement was performed to investigate monoclinic phase zirconium oxide and tetragonal phase zirconium oxide. And the effect of the different chemical composition on the zirconium oxide and the corrosion rate is studied.

## 2. Experimental

### *2.1. Specimen preparation*

Two different types of zirconium alloys, Zr-Nb-Cu and Zr-Nb-Sn alloy plates were used for this research replicating the primary system of pressurized water reactor. The chemical compositions of two specimens are presented in Table 1. The specimen size of Zr-Nb-Sn is 9.5 mm × 15 mm × 0.6 mm, and the specimen size for Zr-Nb-Cu is 10 mm × 10 mm × 0.75 mm, and they are polished before oxidization process. First, the SiC paper is used for polishing from 400 grit to 800 grit. Then, the polishing is conducted using 1 μm diamond paste. Finally, to minimize the mechanical transformation to Zirconium alloy specimens, the 0.05 μm colloidal silica is used for polishing.

### *2.2 Procedure for corrosion experiment in simulated PWR water conditions*

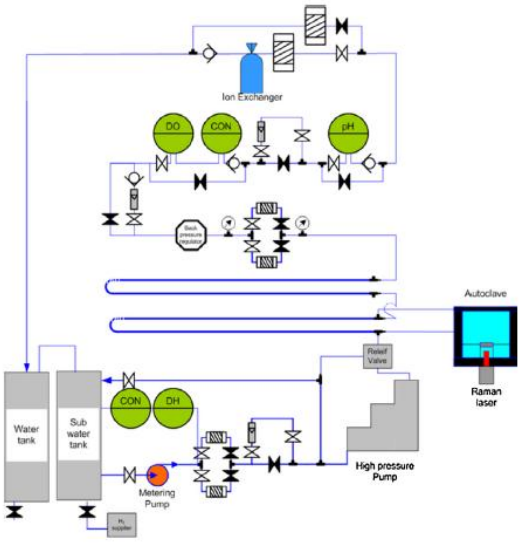


Fig. 1 Total system for corrosion system schematic image

Table. 1 Chemical composition of Zr-Nb-Sn and Zr-Nb-Cu (in wt.%)

| Alloy | Nb | Sn | Hf | Cu | C | O | N | Fe | Zr |
|---|---|---|---|---|---|---|---|---|---|
| Zr-Nb-Sn | 0.96 | 0.76 | 0.002 | - | 0.1 | 0.62 | 0.03 | 0.18 | Bal. |
| Zr-Nb-Cu | 0.55 | 0.06 | - | 0.12 | 0.01 | - | - | 0.07 | Bal. |

For this experiment, the polished Zr-Nb-Cu and Zr-Nb-Sn alloy plates were prepared. To simulate high temperature and high pressure, the loop and autoclave are required. The schematic image of total system for corrosion experiment is following.

Using this simulating system, the primary water chemistry of PWR is set, temperature is 360 ℃, pressure is 19 MPa, dissolved oxygen concentration is under 10 ppb, LiOH and $H_3BO_3$ concentration is 2 and 1200 ppm each. In this experiment, the two Zirconium alloy plate specimens are oxidized in primary water chemistry for 20 days, and the DH concentration is maintained 50 cc/kg.

For oxide analysis, Microstructural characterization was conducted using a Quanta 3D Dual-Beam Focused Ion Beam (FIB) attached to a field-emission gun scanning electron microscope (SEM) with an attached energy dispersive X-ray spectroscope (EDS). And to investigate the monoclinic phase zirconium oxide and tetragonal phase zirconium oxide in the oxide of the zirconium alloys ex situ Raman spectroscopic measurement was performed on the surface of the specimens using Alpha300R with 532nm wavelength ND:YAG laser in 10mW power. And the laser penetration depth is considered to be ~1μm.

## 3. Results and Discussion

### *3.1 Weight gain measurement*

The weight gains of the zirconium alloys in 360 ℃ Li-B water environment for 20 days is shown in Table 2. The weight gain of Zr-Nb-Sn is much larger than that of Zr-Nb-Cu, which means that Zr-Nb-Cu shows better corrosion resistance than Zr-Nb-Sn.

Table. 2 The weight gains of the zirconium alloys in 360 °C Li-B water environment for 20 days

| Alloys | Zr-Nb-Sn alloy | Zr-Nb-Cu alloy |
|---|---|---|
| Weight gain [mg/dm$^2$] | 21.69 | 18.02 |

These results are well matched with the previous researches [2,3]. The corrosion rate of Zr-Nb-Sn alloy is much faster than it of Zr-Nb-Cu alloy. This is because that zirconium alloys exhibit a different corrosion resistance depending on the characteristics of the chemical composition of alloy and its precipitates. The precipitates are oxidized after they are incorporated into the oxide due to the higher resistance of precipitates than zirconium matrix.

### *3.2 FIB-SEM analysis*

To characterize the oxide characteristic, the FIB-SEM analysis was conducted for two oxidized specimens, Zr-Nb-Sn and Zr-Nb-Cu alloy. Figure 2 shows the cross section image of 20 d oxidized specimens, and the Fig. 2 (a) represents the Zr-Nb-Sn alloy and (b) shows the Zr-Nb-Cu alloy cross section.

The oxide thickness of each specimen is measured by SEM and it is compared with the calculated oxide thickness from weight gain results. From the FIB-SEM, the oxide thickness is measured as following; the oxide thickness of Zr-Nb-Cu alloy is 1.06 μm, and the oxide thickness of Zr-Nb-Sn alloy is 1.15 μm. For calculating the oxide thickness from weight gain, and it is assumed that the weight gain is 15 mg/dm$^2$ when the oxide thickness is 1 μm [4]. The calculated oxide thickness of Zr-Nb-Cu alloy is 12.0 μm and it of Zr-Nb-Sn alloy is 14.6 μm. In the Table 3, the information about the oxide thickness is summarized.

Table. 3 Summarized oxide thickness data of zirconium alloy

| Material | Calculated oxide thickness (μm) | Measured oxide thickness (μm) |
|---|---|---|
| Zr-Nb-Cu alloy | 12.0 | 1.06 |
| Zr-Nb-Sn alloy | 14.6 | 1.15 |

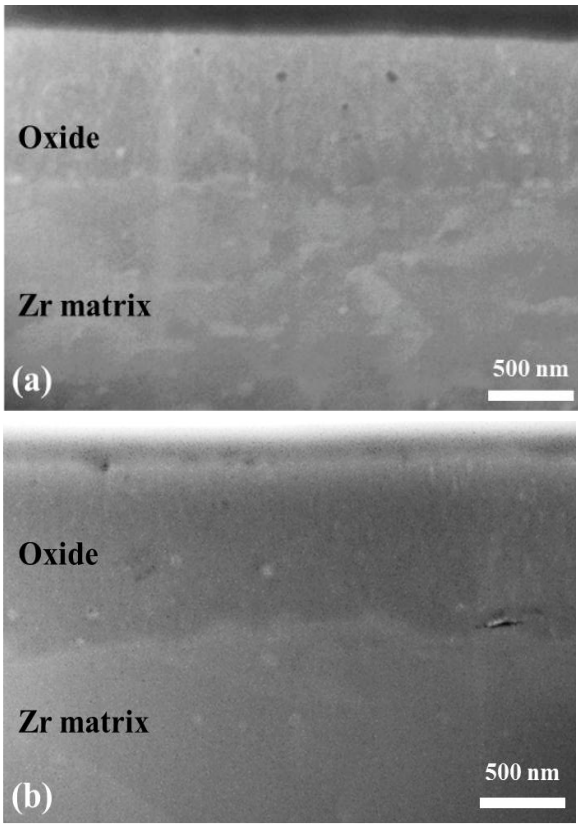


Fig. 2 FIB-SEM image of oxidized zirconium alloy in primary water chemistry for 20 d. (a) Zr-Nb-Cu alloy, (b) Zr-Nb-Sn alloy

These results show that the corrosion resistance is better in the Zr-Nb-Cu alloy than Zr-Nb-Sn alloy. This phenomenon can be explained by the solute elements like tin, niobium, and copper in the zirconium alloy. The high Sn concentration alloy, Zr-Nb-Sn alloy is generally promoting the cracking in the oxide due to the delayed oxidation of segregated elements [2,3]. The delayed oxidation is occurred due to the following process; the Nb and Sn atoms which are dissolved in the zirconium alloy can be segregated in to the oxide grain boundary, and they are finally oxidized when the oxygen potential is high enough for oxidizing the Nb and Sn atoms. Therefore, this process is highly related to the corrosion resistance of zirconium alloy, and can be the evidence of difference of corrosion resistance with the chemical composition of zirconium alloy.

### *3.3 Raman spectroscopy*

In Zr-Nb-Cu alloy oxide, more tetragonal phase zirconium oxide appears than Zr-Nb-Sn alloy oxide. Tetragonal phase zirconium oxide becomes stable when compressive stress exists. By previous study, distribution of compressive stress is highly affected by distribution of precipitates [2,3]. In Nb containing zirconium alloy, the fine β-Nb precipitates which are located in the oxide/metal interface can distribute compressive stress [2,3]. And it delays release of compressive stress so that compressive stress could be distributed in larger oxide/metal interface region [5,6]. Thus it is expected to that the more β-Nb precipitates is distributed, the more tetragonal phase zirconium oxide exist [5,6].

According to the previous researches, Zr-Nb-Cu alloy has more fine β-Nb precipitates than Zr-Nb-Sn alloy [2,3]. Thus, it is expected that Zr-Nb-Cu alloy oxide could have more tetragonal phase zirconium oxide than Zr-Nb-Sn alloy oxide. Ex situ Raman spectroscopic measurement was conducted on the two specimens. Fig. 3 shows that the measured Raman spectrum results of the two zirconium alloys. The Raman spectrum intensity of two specimens is normalized and the monoclinic phase zirconium oxide peak (M) and tetragonal phase zirconium oxide peak (T) is marked. And the detail specification of Raman peak obtained from the two specimens is shown in Table. 4. The peaks located at 177, 224, 308, 380, 474, 503, 616, 639 $cm^{-1}$ show monoclinic phase zirconium oxide of Zr-Nb-Cu alloy oxide and the peaks located at 279, 331, 439 $cm^{-1}$ show tetragonal phase zirconium oxide of Zr-Nb-Cu alloy oxide. The peaks shown at 179, 223, 306, 383, 479, 503, 616, 639 $cm^{-1}$ are attribute to monoclinic phase zirconium oxide of Zr-Nb-Sn alloy oxide and the peaks positioned at 280, 335, 562 $cm^{-1}$ show tetragonal phase zirconium oxide of Zr-Nb-Sn alloy oxide.

Two peaks located at 279 $cm^{-1}$ and 562 $cm^{-1}$ of Zr-Nb-Cu alloy, which appear tetragonal phase zirconium oxide, have stronger intensity than that of Zr-Nb-Sn alloy. And as shown in Fig. 3, more tetragonal phase Raman peak position appears in spectrum of Zr-Nb-Cu alloy oxide than Zr-Nb-Sn alloy oxide, like 439 $cm^{-1}$ peak position.

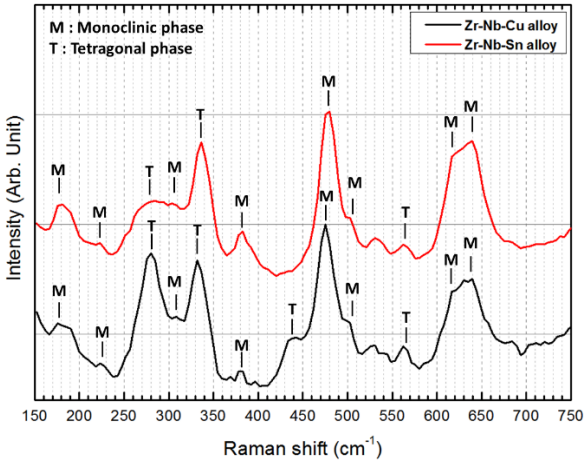


Fig. 3 Measured Raman spectrum of Zr-Nb-Cu alloy and Zr-Nb-Sn alloy oxide excited by a laser at 532 nm at room temperature in air.

Table. 4 Specification of Raman peak position obtained from the two specimens

| Zr-Nb-Cu | | Zr-Nb-Sn | |
|---|---|---|---|
| Monoclinic | Tetragonal | Monoclinic | Tetragonal |
| 177 | | 179 | |
| 224 | 279 | 223 | 279 |
| 308 | 331 | 306 | 335 |
| 380 | | 383 | |
| 474 | 439 | 479 | |
| 503 | | 503 | |
| 616 | 562 | 616 | 562 |
| 639 | | 639 | |

From above Raman spectrum, it is possible to calculate a percentage of tetragonal phase zirconium according to equation (1) [6].

$$\%\ \mathbf{ZrO_2}_{(T)} = \frac{\sum Intensity_{(T)}}{\sum Intensity_{(T)} + \sum Intensity_{(M)}} \quad (1)$$

Table. 5 Calculated percentage of tetragonal phase zirconium oxide.

| Alloy | Zr-Nb-Cu | Zr-Nb-Sn |
|---|---|---|
| % Tetragonal zirconium oxide | 41.2 | 13.8 |

For calculating the summation of the tetragonal intensity 279, 333, 439 $cm^{-1}$ were chosen and for calculation the summation of the monoclinic intensity 178, 474, 616, 639 $cm^{-1}$ were chosen and calculated tetragonal phase zirconium intensity is shown in Table 5. The 178 and 333 $cm^{-1}$ peaks represent the Zr-Zr vibration mode, and the 474 and 616 $cm^{-1}$ peaks can be attributed to the O-O vibration mode.

As shown in Table. 5, the percentage of tetragonal phase zirconium oxide in Zr-Nb-Cu alloy oxide is larger than that of Zr-Nb-Sn alloy oxide. These result are well matched with the expectation that Zr-Nb-Cu alloy has better corrosion resistance than Zr-Nb-Sn alloy, so that

Zr-Nb-Cu alloy has more peak or has stronger intensity tetragonal zirconium oxide peak than Zr-Nb-Sn alloy.

It has been reported that the tetragonal zirconium oxide phase is positioned near the oxide/metal interface and it could act as a barrier layer for oxidizing the zirconium alloy matrix. The stabilization of the tetragonal zirconium oxide can be explained by the high concentration of alloying elements like Cu and Nb, the small grain size and the stresses created by the delayed volume expansion of the precipitate compared to the oxide matrix. It is confirmed from the Raman spectroscopy results show that the tetragonal zirconium oxide fraction is much higher in Zr-Nb-Cu alloy than Zr-Nb-Sn alloy. Due to the alloying elements in Zr-Nb-Cu alloy, the corrosion rate of Zr-Nb-Cu alloy can be slower than it of Zr-Nb-Sn alloy.

As mentioned above, the precipitate has been considered as the key parameter for determining the corrosion rate and corrosion resistance of zirconium alloys. For investigating the precipitates and the cracks effect on zirconium oxidation mechanism, the further TEM analysis will be conducted.

## 4. Conclusion

In this study, the weight gain measurement, FIB-SEM analysis, and Raman spectroscopic measurement were conducted to investigate the effects of dissolved hydrogen concentration and the chemical composition on the corrosion resistance and oxide phase of Zr-Nb-Cu alloy and Zr-Nb-Sn alloy after oxidizing in a primary water environment for 20 d. The corrosion rate of Zr-Nb-Cu alloy is slow, when it is compared to Zr-Nb-Sn alloy. In SEM images, the oxide thickness of Zr-Nb-Cu alloy is measured to be around 1.06 μm it of Zr-Nb-Sn alloy is measured to be 1.15 μm. It is because of the Segregation made by Sn solute element when Sn solute element oxidized. And according to ex situ Raman spectra, Zr-Nb-Cu alloy oxide has more tetragonal zirconium oxide fraction than Zr-Nb-Sn alloy oxide. Tetragonal zirconium oxide is stabilized with compressive stress. Tetragonal phase exists near oxide/metal interface and as the distance from oxide/metal interface increases, monoclinic phase becomes dominant, because compressive stress exists near oxide/metal interface and released as the distance from oxide/metal interface increase.

## ACKNOWLEDGEMENT

This work was financially supported by the International Collaborative Energy Technology R&D Program (No. 20138530030010) of the Korea Institute of Energy Technology Evaluation and Planning (KETEP) which is funded by the Ministry of Trade Industry and Energy.

## REFERENCES

[1] T. Kim, J. Kim, K. J. Choi, S. C. Yoo, J. H. Kim, Phase transformation of oxide film in zirconium alloy in high temperature hydrogenated water, Corrosion Science, pp. 134-144, 2015

[2] J.-Y. Park, B.-K. Choi, S. J. Yoo, Y. H. Jeong, Corrosion behavior and oxide properties of Zr-1.1 wt%Nb-0.05 wt%Cu alloy, Journal of Nuclear Materials, pp. 59-68, 359, 2006

[3] J.-Y. Park, B.-K. Choi, Y. H. Jeong, Y.-H. Jung, Corrosion behavior of Zr alloys with a high Nb content, Journal of Nuclear Materials, pp. 237-246, 340, 2005

[4] M. Oskarsson, E. Ahlberg, K. Pettersson, Oxidation of Zircaloy-2 and Zircaloy-4 in water and lithiated water at 360℃, Journal of Nuclear Materials, pp. 97-108, 295, 2001

[5] L. Kurpaska, J. Favergeon, L. Lahoche, M. El-Marssi, J.-L. Grosseau Poussard, G.Moulin, J.-M.Roelandt, Raman spectroscopy analysis of air grown oxide scale developed on pure zirconium substrate, Jourtnal of Nuclear Materials, pp. 460-467, 466, 2015

[6] L. Kurpaska, J. Favergeon, L. Lahoche, G.Moulin, M. El-Marssi, J.-M.Roelandt, Zirconia layer formed by high temperature oxidation of pure zircoium: stress Generated at the zirconium/zirconia interface, Oxid Met, pp. 261-277, 79, 2013